Applied Energy 375 (2024) 123943

Contents lists available at ScienceDirect

Applied Energy

journal homepage: www.elsevier.com/locate/apenergy

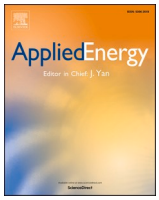

A coreless track-type seamless wireless charging system using co-planar wires enabling quasi-free planar movements for mobile logistics robots

Hyunkyeong Jo, Seoktae Seo, Jungho Kim, Franklin Bien *

Department of Electrical Engineering, Ulsan National Institute of Science and Technology, Ulsan, 689-798, Republic of Korea.

HIGHLIGHTS

- **High System Efficiency:** Achieves 90% efficiency and >100 W power over 16 m without Tx core, the longest coreless track.
- **3-DoF Misalignment Tolerance**: Maintains >82% efficiency with <2% deviation, handling 3-DoF misalignment for dynamic robots.
- **Communication-less Power Feedback System**: Manages power for multiple robots with a communication-less feedback system.
- **Human Safety**: Electromagnetic fields stay within IEEE and ICNIRP safety limits for shared spaces with robots.

ARTICLE INFO

Keywords:
Wireless power transfer
Mobile robot
Coreless transmitter
Seamless charging
Sustainable use of natural resources

ABSTRACT

The adoption of mobile robots in industrial automation is rapidly expanding, driven by not only economic advantages but also considerations for environmental conservation and worker safety. Dynamic wireless power transfer systems for mobile logistics robots emerge as a promising technology, enhancing the feasibility of battery-less mobile robots while concurrently reducing energy and raw material consumptions associated with battery production. Recent research in track-powered mobile robots has advanced the achievement of uniform and reliable power transfer for moving vehicles. In this paper, we introduce an optimally designed transmitter and receiver for seamless charging, affording full degrees of freedom for vehicles within a two-dimensional space. The technique for adjusting the self-resistance of the receiver with a ferromagnetic core has demonstrated a dependable efficiency of nearly 90%, enabling the provision of 100 W of power, sufficient for mobile robot operations. The track length is 16 m, the most prolonged coreless track in the research field. Moreover, we present a communication-less feedback system for multiple vehicles and validate human safety near the robot through simulations and experiments. We anticipate that the proposed wireless charging system will play a fundamental role in promoting the widespread of mobile robots, effectively addressing economic, environmental, and societal challenges.

1. Introduction

Mobile robots, including automated guided vehicles and autonomous mobile robots, are making significant contributions across a wide range of industries, driven by their ability to enhance efficiency and productivity [1]. The desire to minimize virus spread, stemming from the COVID-19 pandemic, has also served as a catalyst, reducing human-to-human interaction and steering towards human-to-machine interaction through the use of mobile robots [2]. Particularly, mobile robots applied in logistics and manufacturing systems offer economic, environmental, and social sustainable benefits, which include (1) cost savings in labor, (2) reduced energy consumption and emissions, and (3) improved safety [3,4]. With a forecast of continued proliferation of mobile logistics robots in the future, there is concern that solutions must be sought to provide adequate power to these huge numbers of units for the sustainability of industrial expansion based on robots [5].

There are two main methods of charging mobile logistics robots: static and dynamic charging. The current method mostly used in the field is static charging, where robots autonomously move to a charging station and utilize metallic contact or wireless charging. The traditional metallic contact method is commonly used because it is easy to implement. However, there is a risk of damage to the terminals due to the physical contact, and it can be challenging to prevent electric shocks in industrial environments with moisture and dust [6,7]. In response to

* Corresponding author.
E-mail address: bien@unist.ac.kr (F. Bien).

https://doi.org/10.1016/j.apenergy.2024.123943
Received 22 December 2023; Received in revised form 7 June 2024; Accepted 14 July 2024
Available online 12 August 2024

these issues, a static charging method using wireless power transmission has been proposed. Particularly, addressing the persistent misalignment sensitivity issue of IPT-based methods with couplers [8–13], control systems [14–17], and compensators [18–20] has increased charging efficiency and reduced the difficulty of robot operation. However, static charging still struggles to overcome the inherent challenges of battery technology. In other words, it requires long charging times and limits the driving range after charging. Furthermore, as the number of robots increases, the need for more charging stations becomes a significant concern.

Another method mentioned above is dynamic charging, which supplies power to moving robots using wireless charging lanes or power tracks. Introducing dynamic charging or dynamic wireless power transfer (D-WPT) to robots can yield three main benefits: (1) Drastically increasing the driving range [21–23], (2) extending lifespan of batteries [24], and (3) enabling the implementation of battery-less robots. The ultimate goal of D-WPT, seamless charging, is one of the most promising technologies alongside energy harvesting that can eliminate batteries in vehicles. Reducing the number of batteries in robots can significantly decrease the consumption of water and energy, as well as alleviate pollutants during the raw material mining process [25]. Additionally, it can offer a method for optimal and sustainable use of limited natural resources. Furthermore, D-WPT can mitigate the drawbacks of Li-ion batteries, such as performance fluctuations in varying environmental conditions [26], making it possible for robots to operate in diverse settings like underwater or extremely low-temperature environments.

The two popular types of D-WPT are the arrayed solenoid type and the track type. The arrayed solenoid type consists of a transmitter (Tx) with multiple coils placed along the pathway of vehicles [27–33]. These solenoid coils typically have a large number of turns and, in most cases, incorporate switches. These devices activate a transmit coil, while the receiver (Rx) is placed among the series of Tx coils. Generally, these systems are expected to achieve high efficiencies of approximately 80–90%. However, this approach carries a critical risk of delivering zero power to the load if the exact position of the Rx is not accurately detected. Furthermore, as arrayed solenoid method is more challenging to extend the charging distance compared to the track type system, it is suitable for rapid charging in short sections within tracks or parking lots.

While the overall efficiency of systems using a track type Tx is slightly lower than that of systems using arrayed solenoids, they do not encounter the problem of power delivery failure [34–37]. Underground wires continuously generate magnetic flux, inducing sufficient voltage on the Rx. To implement seamless charging, high power efficiency must be ensured across every movement of robots in all degrees of freedom (DoF) within planar space. Due to their elongated shape, track type systems have an advantage of maintaining constant efficiency over long distances in the driving direction. However, even in recent research, tolerance to lateral movements is not sufficiently guaranteed, and when approximately half of the vehicle deviates from the track, the efficiency drops to 50% or lower [35,37].

Additionally, considering the actual movements of mobile robots, in-depth considerations are required for robust charging of vehicles with dynamic movements in yaw rotation, as well as longitudinal and lateral movements. The simultaneous power delivery to multiple vehicles should also be explored. Besides, Tx core structure used by most track type systems can become an obstacle when applied in real-world settings. Since mobile logistics robots need to move heavy loads, solutions are needed to address the brittle characteristics of ferrite cores in the floor. The charging method for multiple vehicles on the track also should be explored and demonstrated.

In this study, we introduce a wireless charging track system designed for mobile logistics robots, featuring a ferromagnetic-coreless Tx. The Tx, composed of multiple co-planar wires, ensures robust efficiency during dynamic vehicle movements. Unlike the typical track-type system that picks up power using only z-directional magnetic field at the center of the loop, our system utilizes the omni-directional field at the edge. Therefore, we have designed a Rx suitable for capturing power from this flux. We tested that the system maintains high efficiency and stable power delivery even when the vehicle exhibits 3-DoF movements on a square track of 16 m. Power exceeding 100 W, which is sufficient to support the operation of the running robot, were delivered to the Rx to verify the performance of the proposed system. Additionally, power feedback without communication for multiple vehicles and human safety were conceived and demonstrated experimentally.

The key contributions of this work include the following aspects.

- The proposed system provides the highest efficiency, misalignment tolerance, and driving range compared to existing D-WPT systems, even without a Tx core (Supporting Table 1).
- Seamless wireless charging is demonstrated, enhancing the feasibility of implementing a battery-less mobile robot.
- Charging for multiple robots with communication-less power feedback when robots enter or exit the track was demonstrated.
- When workers pass by the robot, the exposure to electric and magnetic fields is minimal, satisfying IEEE [38] and ICNIRP safety standards [39].

The rest of this paper is organized as follows: An introduction to the system's overview and working principle is provided in Section 2. Section 2 also covers the methods for designing and optimizing the Tx and Rx. Section 3 presents the experimental verification of the optimized system. Power feedback systems without communication between the Tx and Rx are detailed in Section 4, and Section 5 reports on the safety assessment for human co-workers. The main conclusions and discussions are presented in Section 6.

2. System design

2.1. Overview of the proposed system

2.1.1. Working principle

The mobile logistics robots deployed in logistics warehouses serve the role in goods-to-person operations. In this context, as shown in Fig. 1, these vehicles move not only longitudinally but also laterally to navigate around obstacles and follow the optimal path for tasks. In addition, they also rotate their bodies to change direction. Therefore, wireless charging tracks designed for mobile logistics robots should guarantee alignment tolerance for movements in 3-DOF to provide robust charging. In this paper, the longitudinal and lateral directions represent the x- and y-directions, respectively, in Cartesian coordinate.

The proposed system is designed to use the going and return paths of current separately during the power acquisition process. Therefore, as depicted in Fig. 2 (a), by effectively capturing the magnetic flux formed by Ampere's law, a coil-structured Rx integrated into the robot can supply a sufficient amount of power to the vehicle in motion. An AC moving through a long and straight wire induces a circular magnetic field around the wire (Fig. 2 (b)). Because the partial derivative of the intensity of the field for y is zero, the straight wire acting as Tx can provide longitudinal tolerance to the proposed system. However, a Tx composed of a single wire still delivers variable power with respect to the relative position between the wire and Rx. Therefore, parallelly linked cascaded cables shown in Fig. 2 (c) are employed to generate uniform distribution by merging the magnetic fields from each wire.

Table 1
The performance evaluation of the proposed track type wireless power transfer system.

Direction	Max. displacement	Max. efficiency	Min. efficiency
Longitudinal (x)	4 m		87%
Lateral (y)	0.25 m	90%	82%
Yaw rotation	60°		82%

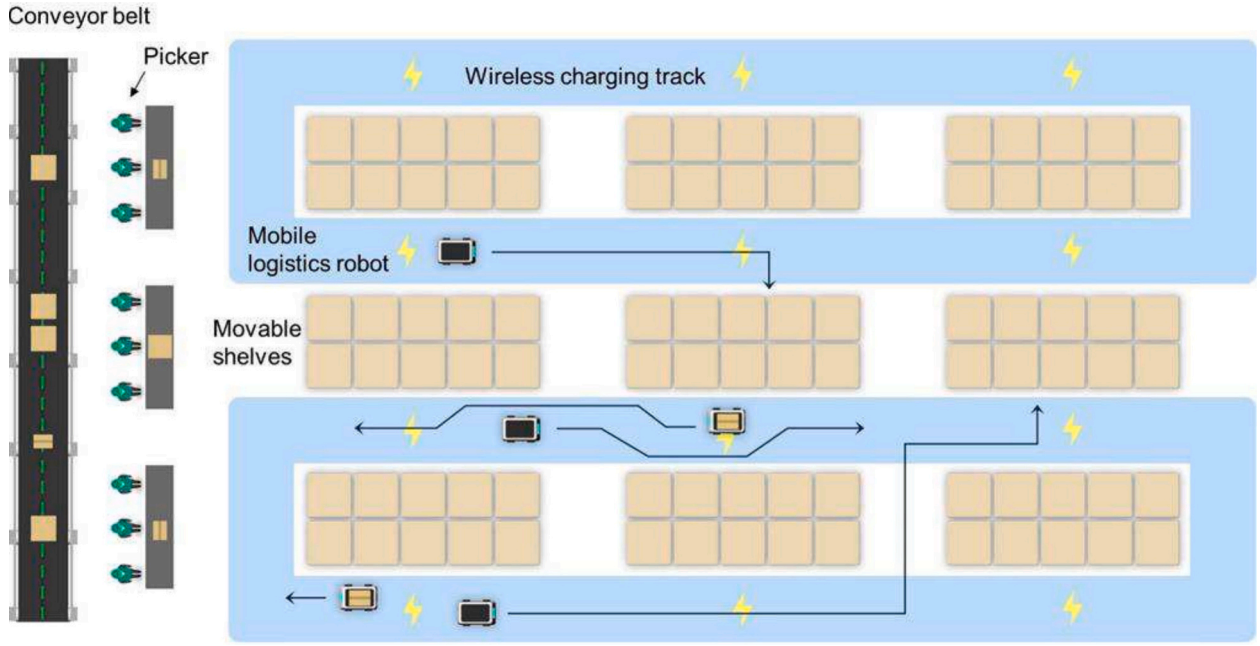

Fig. 1. Application of a track type dynamic wireless power transfer system in logistics.

2.1.2. Comparison with the general track type

The Tx shape of the track type, including the proposed system, can be approximated as a rectangular closed loop (Fig. 3 (a)). In this case, the magnetic field in the z-direction (H_z) at an arbitrary point **P** on the loop can be obtained by the superposition of magnetic fields generated by the four components forming the loop. The magnetic fields produced by each component, calculated using Biot-Savart's law, and the merged magnetic field are as follows.

$$H_{1z} = \frac{I}{4\pi}\frac{D_1/2-x}{(D_1/2-x)^2+z^2}\left(\frac{D_2/2-y}{(D_1/2-x)^2+(D_2/2-y)^2+z^2}+\frac{D_2/2+y}{(D_1/2-x)^2+(D_2/2+y)^2+z^2}\right) \quad (1)$$

$$H_{2z} = \frac{I}{4\pi}\frac{D_1/2+x}{(D_1/2+x)^2+z^2}\left(\frac{D_2/2-y}{(D_1/2+x)^2+(D_2/2-y)^2+z^2}+\frac{D_2/2+y}{(D_1/2+x)^2+(D_2/2+y)^2+z^2}\right) \quad (2)$$

$$H_{3z} = \frac{I}{4\pi}\frac{D_2/2-y}{(D_2/2-y)^2+z^2}\left(\frac{D_1/2-x}{(D_1/2-x)^2+(D_2/2-y)^2+z^2}+\frac{D_1/2+x}{(D_1/2+x)^2+(D_2/2-y)^2+z^2}\right) \quad (3)$$

$$H_{4z} = \frac{I}{4\pi}\frac{D_2/2+y}{(D_2/2+y)^2+z^2}\left(\frac{D_1/2-x}{(D_1/2-x)^2+(D_2/2+y)^2+z^2}+\frac{D_1/2+x}{(D_1/2+x)^2+(D_2/2+y)^2+z^2}\right) \quad (4)$$

$$H_z(x,y,z) = H_{1z}+H_{2z}+H_{3z}+H_{4z} \quad (5)$$

As typical track type system picks up z-direction magnetic flux within a closed loop ($-D_1/2 < x < D_1/2$, $-D_2/2 < y < D_2/2$), generally D_2 is made significantly shorter than D_1 to increase the magnetic field intensity. Since the power is delivered simultaneously from two components of the loop, the driving range does not extend beyond half of the loop's perimeter, which may increase the Tx resistance.

In comparison, the proposed system employs the magnetic fields generated by each component in proximity. Fig. 3 (b) shows the intensity of H_z along the y-directional movement of the observing point with $x = 0$. A strong but highly deviating field is formed at the edge of the loop, while a relatively weak and consistent field is formed at the center. As the proposed system does not employ a ferrite core at the Tx, the strong field near the wire should be incorporated into the system to enhance the cross-coupling between Tx and Rx. Then, both Tx and Rx must be optimized to obtain uniform power, even with movement of Rx. Especially, it must be considered that, unlike the existing system, H_y has a significant magnitude due to D_2 being comparable with D_1. Thus, in the following sessions, we designed and verified an Rx and Tx that can supply constant power regardless of the robot's movement in any direction.

2.2. Design and optimization of the receiver

2.2.1. Design of the core structure

The operating frequency was set to 20 kHz according to the frequency range recommended by ITU-R/SG [40]. The coupling between Tx and Rx is affected by the geometry of the system, that is, distance, dimension, and shape. In the proposed system, the cascaded wires such as Tx barely have complex geometric parameters, unlike Rx. The length of Tx was set to 4 m (one side of the track), according to the limited laboratory conditions. The dimensions of Rx, such as length and width,

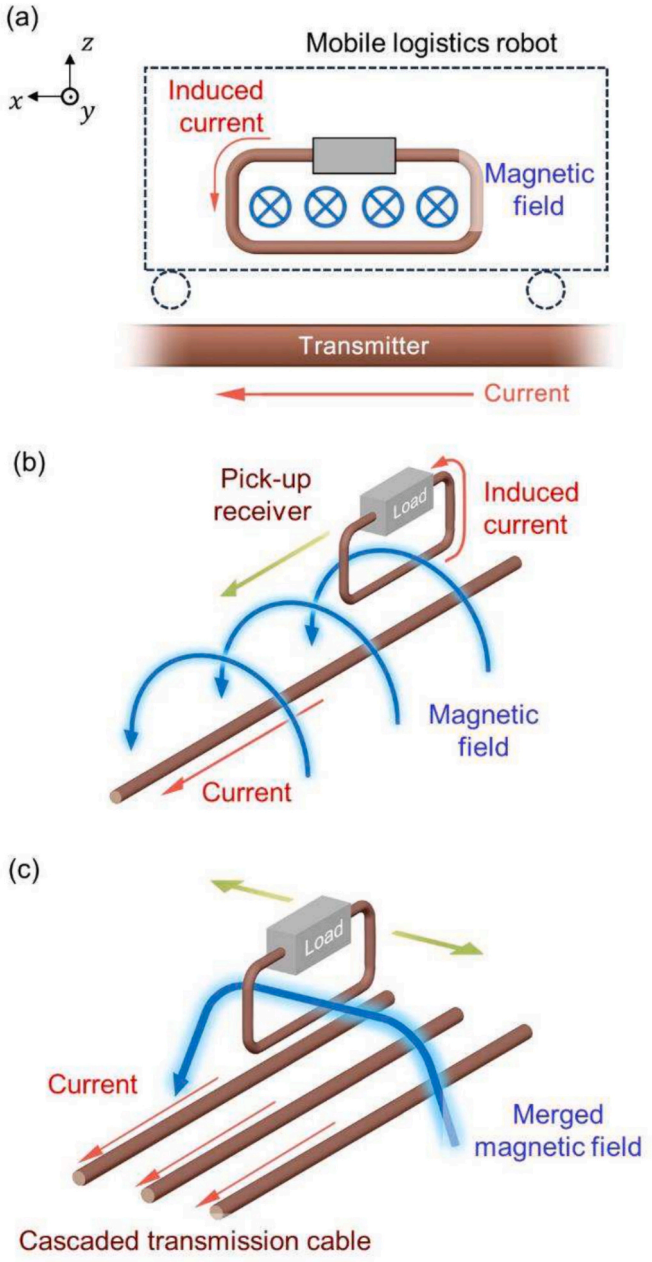

Fig. 2. System overview and working principle. (a) Principle of picking up power at the receiver. (b) Transmission line with a pick-up coil. (c) Proposed track type charging system for lateral displacement.

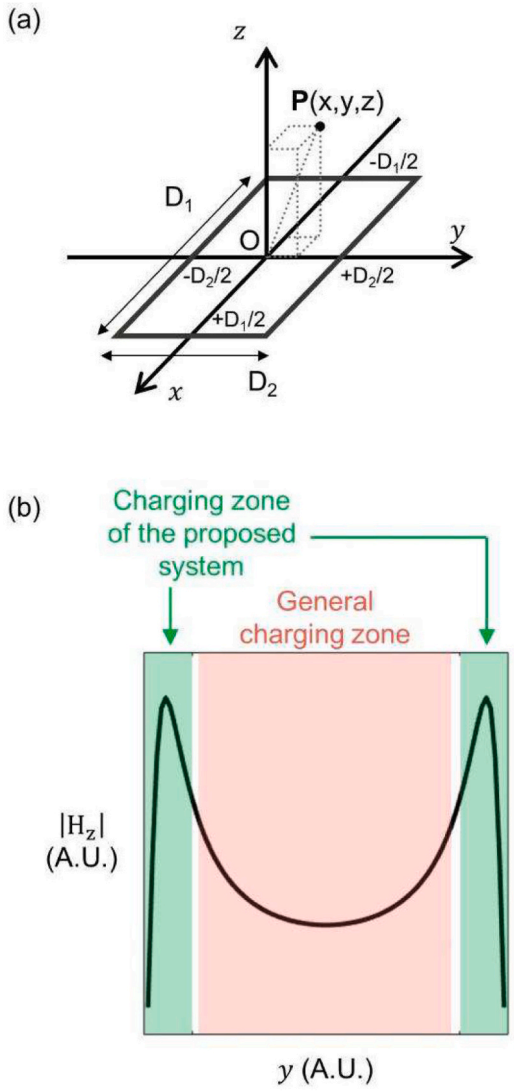

Fig. 3. Comparative analysis of charging zone in the proposed and general track type WPT systems. (a) Structure of the track type WPT. (b) Vertical magnetic field intensity from the rectangular loop.

were set to 50 cm, considering those of commercial vehicle models.

A ferrite core was adopted for Rx, and wires were wound around the core. On the extended and linear track, the partial derivative of magnetic field in x-direction is zero. Therefore, power transfer efficiency remains robust during the longitudinal movement of the vehicles with the flat core. The efficiency during rotation, however, varies based on the relative angle between the magnetic flux vector and normal vector of the receiving coil, as received power is proportional to the inner product between two vectors. To address this issue, two core legs were introduced to enhance magnetic flux induction into Rx by capturing the vertical component. Since the normal vectors of the legs are consistently aligned with the $\mathbf{H_z}$ of the proposed system which has strong intensity as shown in Fig. 3 (b), the efficiency variation during yaw rotation can be regulated.

Before fixing the Rx design, a verification was conducted using a single Tx wire placed in the middle of the Rx core. Fig. 4 (a) show three possible ferrite core-shape candidates: flat, U-beam, and H-beam models. The magnetic flux density was simulated through finite-element analysis using Ansoft Maxwell v14.0 (Fig. 4 (b)). The simulation verified that the core leg enhanced the inner magnetic flux of Rx. The implemented Rx are shown in Fig. 4 (c). USTC wires were adopted for all wires, including the Rx windings and Tx lines, to minimize the skin effect and AC resistances. The Ni-Zn-type soft ferrite material SN-20 was acquired from Samwha Electronics, Korea. The core thickness was determined in multiples of 0.7 cm, as the smallest available material size was 5x5x0.7 cm^3. Considering the application, the core body thickness was set to 1.4 cm to ensure it is not too thick while still effectively.

capturing voltage from horizontal flux. As for the legs, which act as guides for vertical flux, they were designed to have the minimum volume to ensure a fair comparison with the flat model. The core body was located 17 cm above the Tx wire.

The experimental conditions are shown in Fig. 5. The mutual inductances and efficiencies were studied for each Rx while moving from 0.5 m to 3 m in 0.5 m intervals along the longitudinal direction. Because the system assumes a sufficiently long transmission wire, data at 0 m and 3.5 m, where the edge of Rx reaches the end of the wire, were not

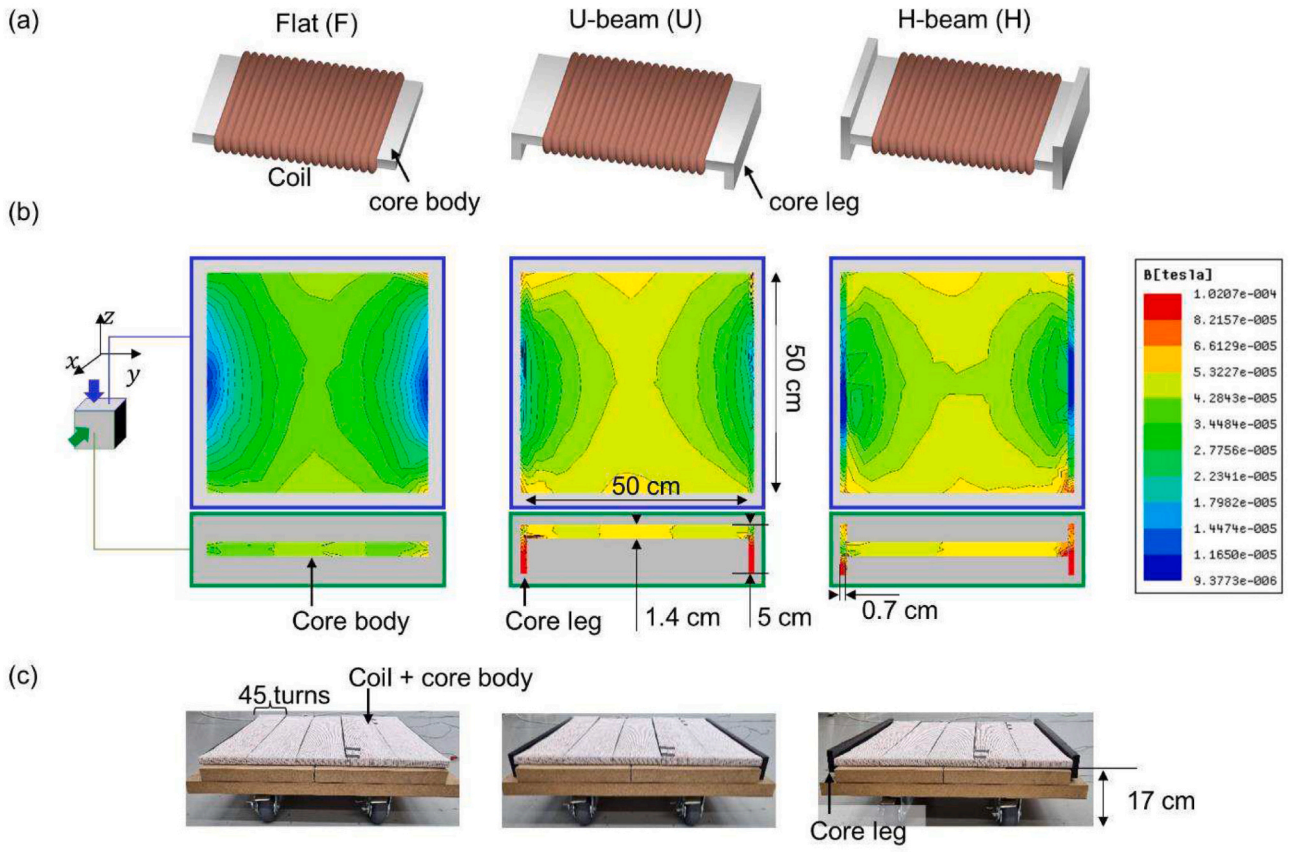

Fig. 4. Three candidates of core structures for stable efficiency in longitudinal movements of receivers. (a) Conceptual designs for the receiver structures. (b) Inner magnetic flux simulation for three ferrite core shapes. (c) Fabricated receivers.

considered. Validation was carried out for one of the four sides, given the symmetry of the track.

Mutual inductance is an expression of the coupling between Tx and Rx based on the transformer model (Fig. 6). When the current, I_S, does not flow through Rx (Rx is open), the open voltage at Rx, V_S, is decided by Eq. (6).

$$V_S = \omega M I_P, \tag{6}$$

where ω is the frequency in radians, M is the mutual inductance, and I_P is the total current flowing through Tx. Thus, the mutual inductance can be calculated using Eq. (7).

$$M = \frac{V_S}{\omega I_P} \tag{7}$$

To obtain the efficiency, the system is modeled by the circuit in Fig. 7. A time-varying magnetic field induces a 90-degree phase-shifted current in adjacent wires. In this study, straight Tx wires induced a current in the coiled Rx with a load R_L. The induced current appears to be a current-controlled voltage source for Rx. The current through Rx generates the time-varying magnetic field, which induces a completely out-of-phase current in the Tx wires if Rx resonates [41] (Supporting Note 1). The completely out-of-phase current causes a voltage drop at Tx as well as the self-impedance of Tx. The ratio between the total voltage drop at Tx and the Tx currents can be described as the impedance, which is the reason the ratio is called the reflected impedance Z_{in}. Thus, the reflected impedance can be used to interpret the entire system by observing Tx parameters.

The proposed system compensates for the inductances of Tx and Rx with serial capacitors. Eq. (8) shows the reflected impedance at Tx with a single Rx.

$$Z_{in} = \frac{V_P}{I_P} = R_P + \frac{(\omega M)^2}{(R_S + R_L)} \tag{8}$$

Then, the efficiency(η) is defined as Eq. (9).

$$\eta = \frac{R_L I_S}{Z_{in} I_P} \tag{9}$$

The efficiencies in the main text are calculated from Eq. (9) with a tolerance of <2% (Supporting Note 2). The induced current at Rx can be described in terms of the Tx current (Eq. (10)).

$$I_S = -j\omega M \frac{\frac{I_P}{(R_S+R_L)}}{(R_S + R_L)} \tag{10}$$

Thus, the efficiency is formulated as Eq. (11).

$$\eta = -j\omega M \frac{R_L}{Z_{in}(R_S + R_L)} = \frac{R_L}{(R_S + R_L)\left(1 + \frac{(R_S+R_L)}{(\omega M)^2} R_P\right)} \tag{11}$$

From Eq. (11), the maximum efficiency at the optimal load $R_{L,opt}$, can be derived as Eq. (12) using the first derivative of the efficiency about R_L.

$$R_{L,opt} = R_S \sqrt{1 + \frac{(\omega M)^2}{R_S R_P}} \tag{12}$$

With the optimal load, the optimal system efficiency is obtained by Eq. (13).

$$\eta_{opt} = \frac{R_{L,opt} I_S}{Z_{in} I_P} = \frac{R_{L,opt} I_S}{R_P I_P + (R_S + R_{L,opt}) I_S} \tag{13}$$

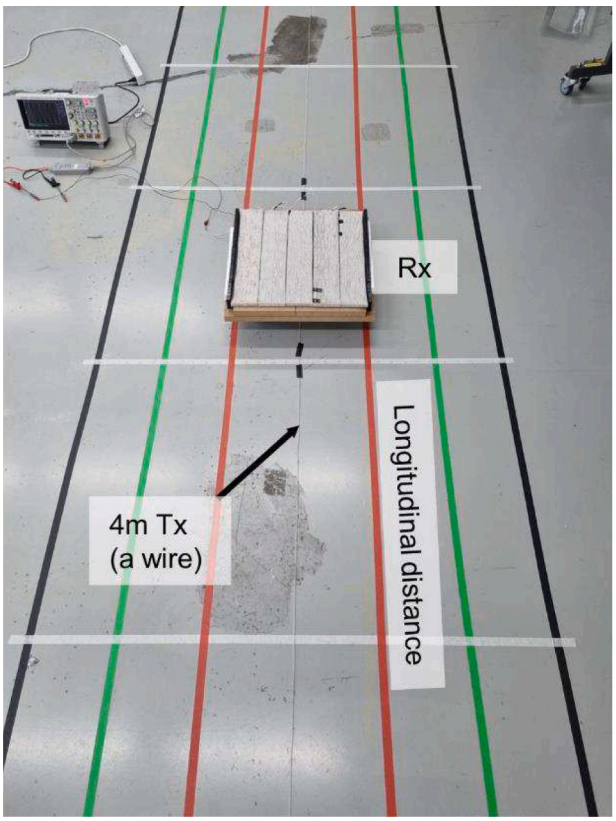

Fig. 5. Experimental conditions for longitudinal stability of three candidates of receivers.

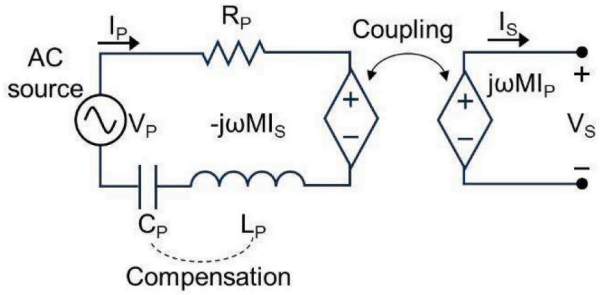

Fig. 6. Transformer circuit model of the system with a single receiver.

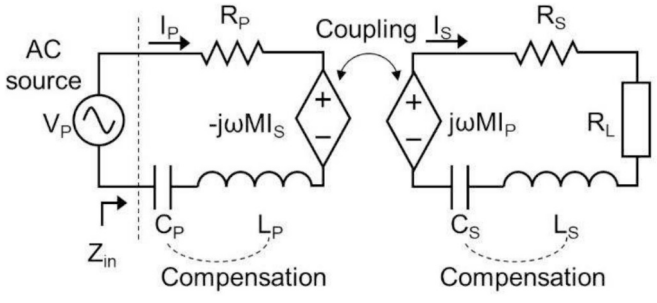

Fig. 7. Circuit model of the proposed dynamic wireless power transfer system.

The experiments are designed to find the model with the most consistent efficiency in the longitudinal direction, considering the shape of the core as a control variable. The difference between the maximum and minimum efficiency is tiny, so the standard deviation is suggested as a variable to express the stability of the efficiency against the vehicle's movement. As shown in Fig. 8, the H-beam model exhibited the highest average efficiency and lowest standard deviation of the efficiency. This indicates that Rx with the H-beam core is more resilient to misalignment than the other models. Based on the simulation and experimental results, it is clear that the H-beam core suits the Rx shape.

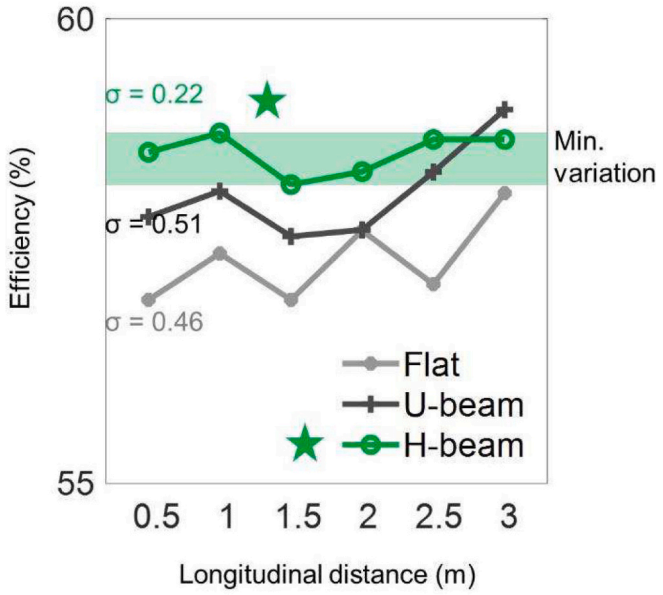

Fig. 8. Experimental results for longitudinal efficiencies of three receivers with standard deviations (σ).

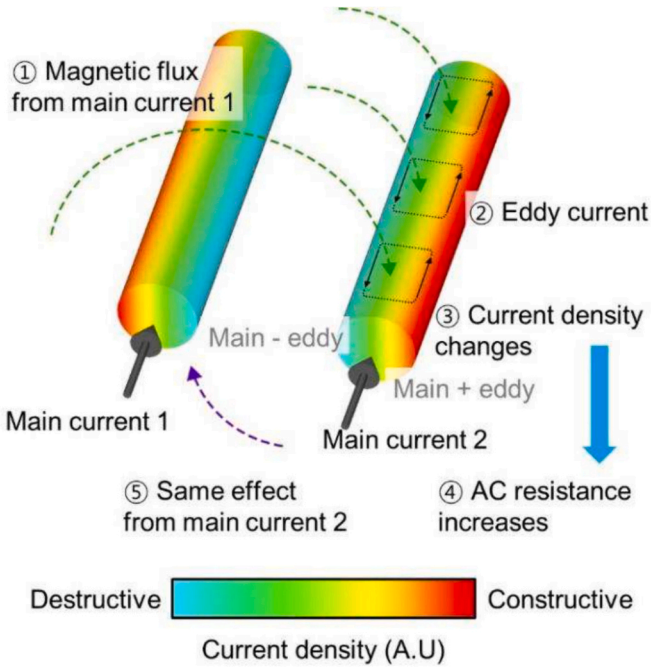

Fig. 9. A mechanism of the rise of the AC resistance between adjacent wires.

2.2.2. Enhancing efficiency by reducing eddy current from leakage flux at the receiver

A remaining challenge is the low efficiency caused by the high AC resistance of Rx. Fig. 9 shows the mechanism of a surge in the Rx

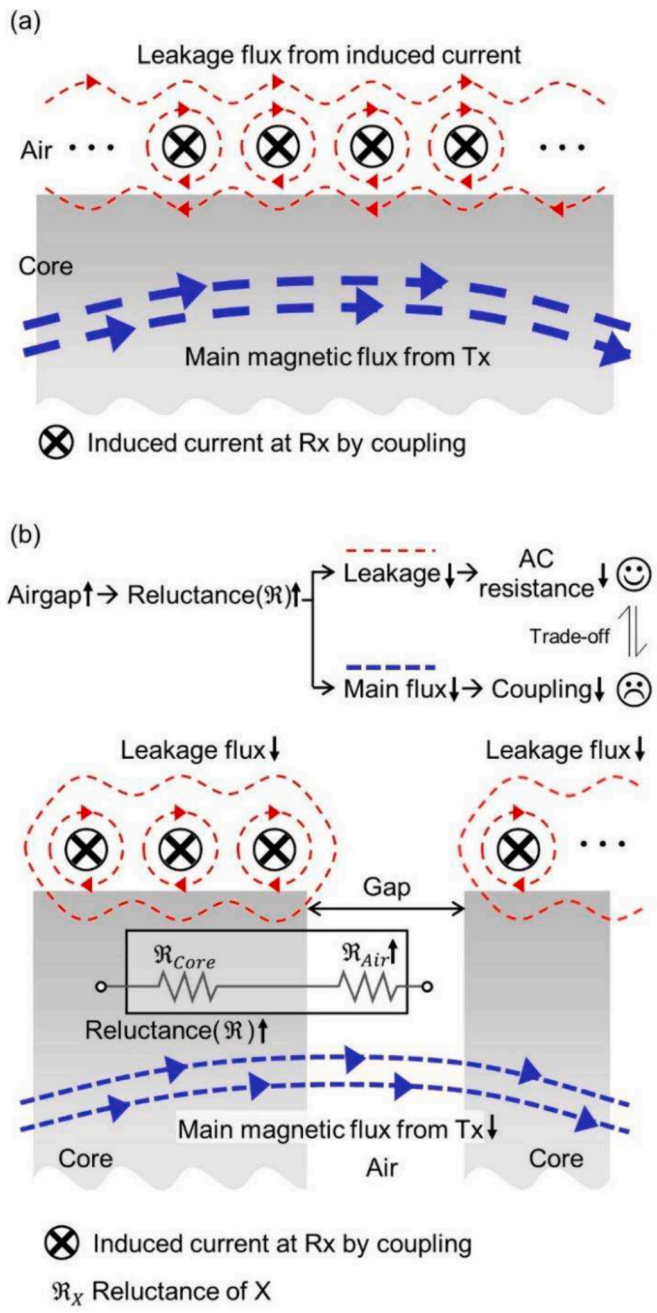

Fig. 10. The impact of ferrite core (a) without and (b) with air gaps on the AC resistance of the receiver.

resistance of the proposed system. Consider two parallel wires carrying currents in the same direction, denoted as Main current 1 and 2 in Fig. 9. In this scenario, Main current 1 induces magnetic flux in the adjacent wire. This flux generates eddy currents in the wire, pushing them in the direction to oppose the flux. These eddy currents interact with Main current 2, causing both destructive and constructive interference in the wire, resulting in non-uniform current density within the wire. As a consequence, this phenomenon leads to an increase in AC resistance, meaning that more power needs to be supplied to maintain the same current. This effect occurs similarly by Main current 2 as well, so both closely positioned wires experience an increase in AC resistance due to the non-uniform current density [42,43]. In the proposed system, the induced current in the Rx coil, resulting from the picked-up power, causes a similar phenomenon. The leakage flux generated from this induced current generates eddy currents in adjacent wires, thereby increasing AC resistance of the Rx.

The ferrite core with high permeability intensifies the magnetic flux passing through the Rx coils, thereby increasing the pick-up power. However, it can also simultaneously amplify the leakage flux of the induced current (Fig. 10 (a)). Also, since the amplified main flux increases mutual inductance between Tx and Rx through the core, the eddy current in the Rx coil increases, interfering with the total current flow. As shown in Fig. 10 (b), raising reluctance through an air gap with low relative permeability can impede leakage flux and reduce AC resistance. Nevertheless, there is an efficiency trade-off, as mutual inductance due to the main flux also decreases. Therefore, optimizing the Rx structure can be achieved by adjusting the gap between the cores and conductors of the Rx wires.

The number of conductors and the spacing between them were adjusted to reduce the self-resistance of Rx, as illustrated in Fig. 11 (a). Introducing a gap between the core bodies, as shown in Fig. 11 (b), is also valid for mitigating AC resistance. If the gap is significantly large, the eddy current by the leakage flux almost disappears, but the mutual inductance is greatly reduced such that no power is transmitted. The optimal number of pick-up coils and air gap were determined based on the experimental results. Consequently, the system efficiency with the single Tx wire increased drastically from 58.6% to 75.8% through optimization using three conductors and 2-mm-gap.

2.3. System optimization for reliable efficiency over lateral direction

Because the intensity of the magnetic field generated by a straight wire is a function of the distance between the observation point and the center of the wire, Tx should adopt multiple wires to provide uniform power despite lateral displacement (Fig. 12 (a)). An increase in the number of parallel wires in Tx reduces the Tx resistance, thereby improving the system efficiency. However, many wires in a limited area elevate self-resistance, disturbing the even distribution of the current through the cascaded wires. Thus, the optimal number of Tx wires was studied.

The simulation and experimental conditions are given in Fig. 12 (b). The width of each lane was 1 m, and the Tx wires were uniformly placed within a 50 cm range. Rx moved from −25 cm to +25 cm in increments of 5 cm in the lateral (y) direction. Assuming that the proposed system is sufficiently long, Tx structure can be projected into two dimensions, as shown in Fig. 12 (c). There are n co-planar wires and the total current I flows evenly distributed to each wire into the slide. The distance between the k^{th} wire and the observing point is presented r_k and the angle between them is Θ_k. The space between the k^{th} and k + 1th wires is L_k. Using Biot-Savart's law, $\mathbf{H_y}$, $\mathbf{H_z}$, and $\mathbf{H}$ are calculated as follows.

$$\mathbf{H}_y(y) = \frac{Ih}{2\pi n}\sum_{k=1}^{n}\frac{1}{\left(x-\sum_{i=1}^{k-1}L_i\right)^2+h^2} \tag{14}$$

$$\mathbf{H}_z(y) = -\frac{\mathbf{I}}{2\pi n}\sum_{k=1}^{n}\frac{\left(y-\sum_{i=1}^{k-1}L_i\right)}{\left(y-\sum_{i=1}^{k-1}L_i\right)^2+h^2} \tag{15}$$

$$\mathbf{H}(y) = \mathrm{H}_y(y)\hat{\boldsymbol{y}} + \mathrm{H}_z(y)\hat{\boldsymbol{z}}, |\mathbf{H}(y)| = \sqrt{\mathrm{H_y}^2+\mathrm{H_z}^2} \tag{16}$$

The distribution of the field intensity changes as the number of wires increases (Fig. 12 (d)). A significant decrease in standard deviation with three or more wires was confirmed through the simulation. Also, the experiment to investigate the optimal number of Tx wires was conducted. The mutual inductances were measured with different numbers of Tx wires ranging from two to eight. Fluctuation ranges and standard deviations were observed to compare the differences between the maximum and minimum values and the overall distributions of the expected pick-up power at the Rx, respectively. The fluctuation range is formulated by the eq. (17) [12], where $V_{S,max}$ and $V_{S,min}$, which represent

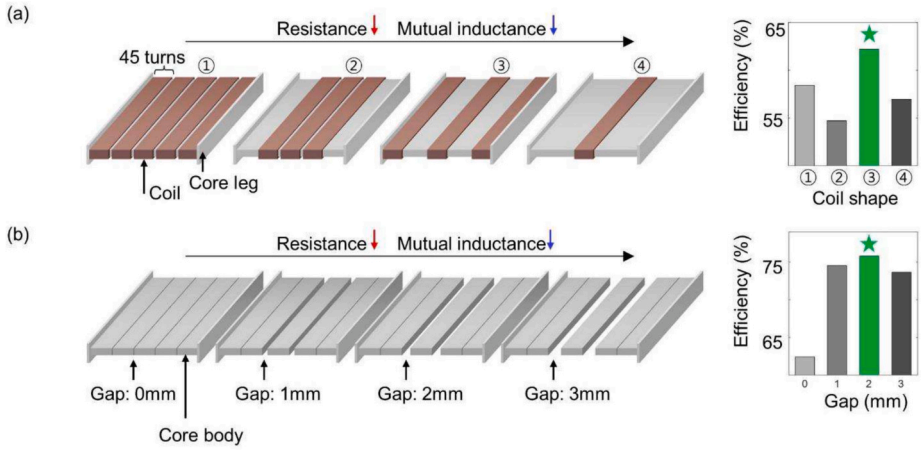

Fig. 11. Experimental results for receiver optimization. (a) Efficiency improvement method 1: adjustment of conductor distribution and its result. (b) Efficiency improvement method 2: adjustment of core gap and its result.

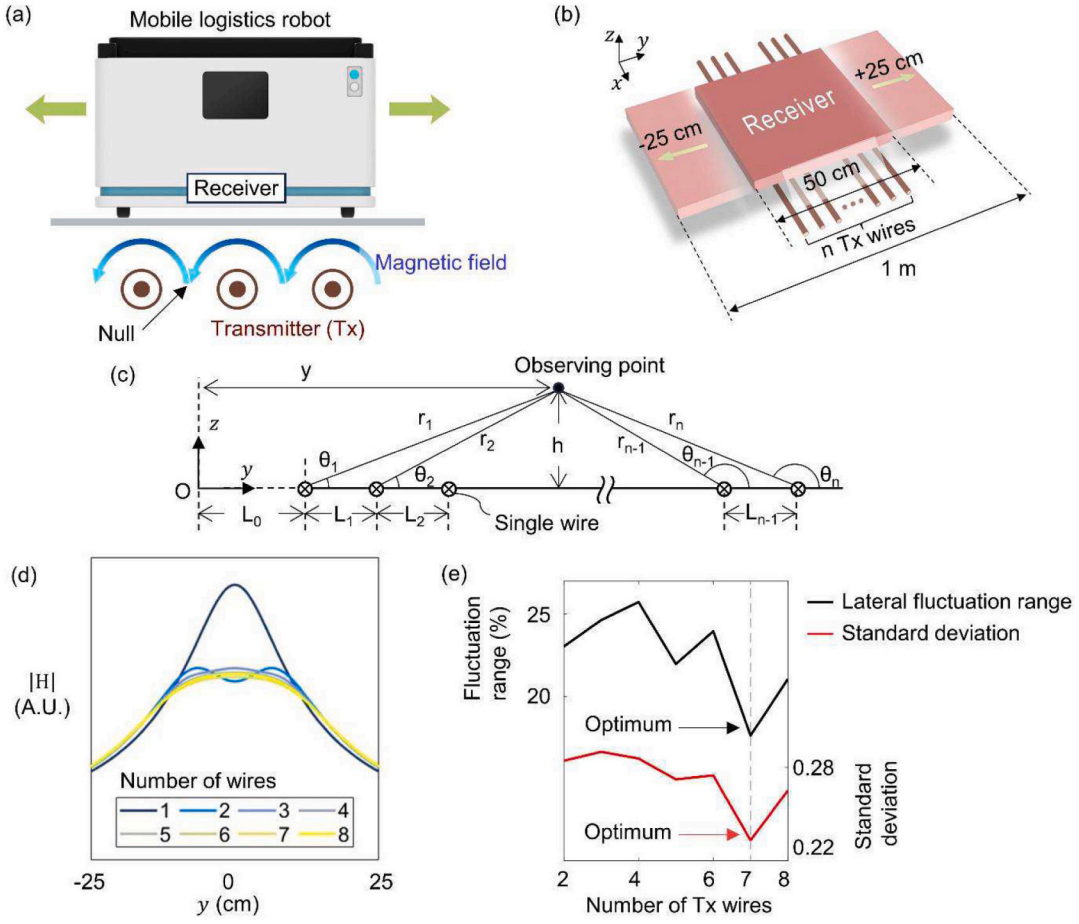

Fig. 12. Optimization of transmission wires for stable power transfer along lateral displacement for vehicles. (a) Circular magnetic fields generated by the transmission wires and lateral movement of the vehicle. (b) Experimental conditions to determine the optimal number of transmission wires for lateral stability. (c) A projection of the proposed system. (d) Simulated magnetic field intensity with various number of Tx wires. (e) Experimental results on lateral fluctuation with different numbers of wires.

the maximum and minimum open circuit voltages at Rx, respectively.

$$\text{Fluctuation range} = \frac{V_{S,max} - V_{S,min}}{V_{S,max} + V_{S,min}} \tag{17}$$

As shown in Fig. 12 (e), the criteria are at a minimum when the number of wires is seven, which means that the system has the best misalignment tolerance in the lateral direction with small variations.

3. Results: Validation for misalignment tolerance in 3-DoF

Fig. 13 (a) shows the fabricated system after optimization. Serial capacitors and resistors are connected to the Rx to provide

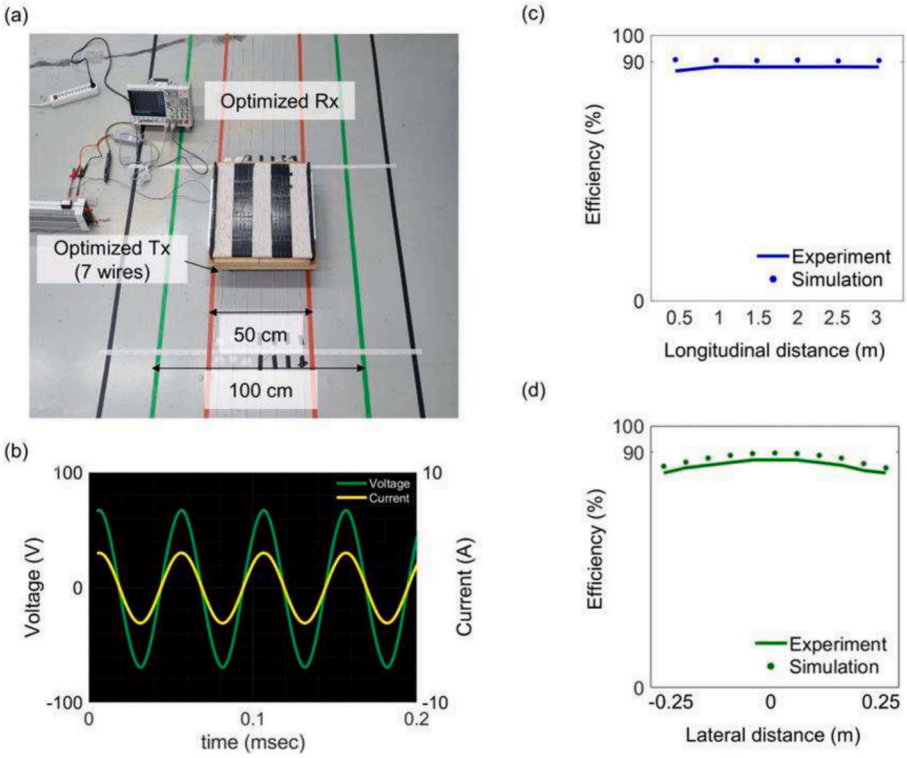

Fig. 13. Experimental validation of the proposed track type wireless power transfer system. (a) Experimental setup with the optimized system. (b) Experimental results for the maximum pick-up power (c-d) Uniform efficiencies from the simulations and experiments along the longitudinal and lateral movements.

compensation and optimal load conditions, respectively. To verify the system, the pick-up powers and efficiencies were acquired while moving the Rx along the longitudinal and lateral directions, and the results are shown in Fig. 13 (b–d). Maximum power >100 W was transferred to load. Although the efficiencies from the experiment show a little difference with those from simulation (around 3%p), uniformly high efficiencies of approximately 90% were achieved regardless of the longitudinal Rx position with very low fluctuation range (< 1%). Also, the efficiency along the lateral movement was also verified, varying from 82% to 88%.

Tolerance to angular displacement was also discovered. Fig. 14 shows that the power efficiencies vary with the angles between the Tx wires and Rx from 0° to 180°. The efficiency approached zero at 90° but remained high in the other cases, consistently exceeding 84%. When the vehicle passes through the curved section of the track, there are very few instances where the relative angle between the vehicle and the track reaches exactly 90°. These moments are brief, and the stored energy in the battery is not fully utilized during such occurrences. Consequently, it has been confirmed that the proposed system provides misalignment tolerance to 3-DoF movements (lateral, longitudinal, and angular displacements) when high power is transferred.

Up to 90.03% of the total power is delivered to the load, while the remaining power is consumed by AC loss, DC loss, and core loss. Losses are classified into DC loss, AC loss, and core loss. The Tx cable and Rx coil each have DC loss (conduction loss) and AC loss caused by skin and proximity effects. The core included in the Rx unit has core loss, which is a combination of hysteresis, eddy current, and residual losses. DC resistance and AC resistance were measured using an LCR meter (Good Will Instrument Co., Ltd., LCR-6200). Measuring core loss is extremely challenging, so it was calculated by subtracting the measured losses in the overall loss. The analysis result can be found in Fig. 15.

4. Feedback system for multiple receivers

More than one vehicle drives in a track, and newly arrived vehicles are added to that track. Because the power to be supplied varies with the number of vehicles, the proposed system must identify the number of vehicles and provide power feedback. However, the communication between a controller and Rx consumes additional power, which reduces the system efficiency. On the Rx side, which operates various functions such as motor driving, cooling, and computing with limited battery capacity, reducing power consumption in any way can be beneficial. To address this issue, a source power control based on a reflected impedance (Z_{in} in Fig. 16) without communication is proposed.

The linkage between transmitter (Tx) and receiver (Rx) involves various variables, but if the system structure, constituent materials, and medium do not change, the mutual inductance between them is most influenced by the magnetic flux intensity from the Tx. Since magnetic flux intensity is proportional to current, we proposed this controller based on the principle that the coupling between Tx and Rx can be maintained without communication if the current of the Tx (I_p) is controlled to be constant. Fig. 16 (a) shows the circuit model of multiple vehicles (Rx) on the charging track (Tx). If a new vehicle arrives, the new coupling between Tx and the newly arrived Rx generates a counter electromotive force on the Tx wires, which leads to an increase in the reflected impedance and a drop in the current through the Tx wires. Therefore, the Tx current can be used as an input variable to control the power source and conventional techniques such as PID, time delay control, or AI-based control can all be applied to the suggested controller as a current regulator, as shown in Fig. 16 (b).

The proposed WPT method is a SIMO system, but if there is no undesirable coupling between the Rx units, it can be seen as an individual SISO system for each Rx. Therefore, this controller applies equally to each Rx and Tx even if the number of Rx units increases. At that time, assuming the internal resistances of the Rx units (R_S) are identical, the reflected impedance (Z_{in}) is expressed below.

$$Z_{in} = R_P + \frac{(\omega M_1)^2}{(R_S + R_{L1})} + \frac{(\omega M_2)^2}{(R_S + R_{L2})} + \ldots + \frac{(\omega M_N)^2}{(R_S + R_{LN})} \tag{18}$$

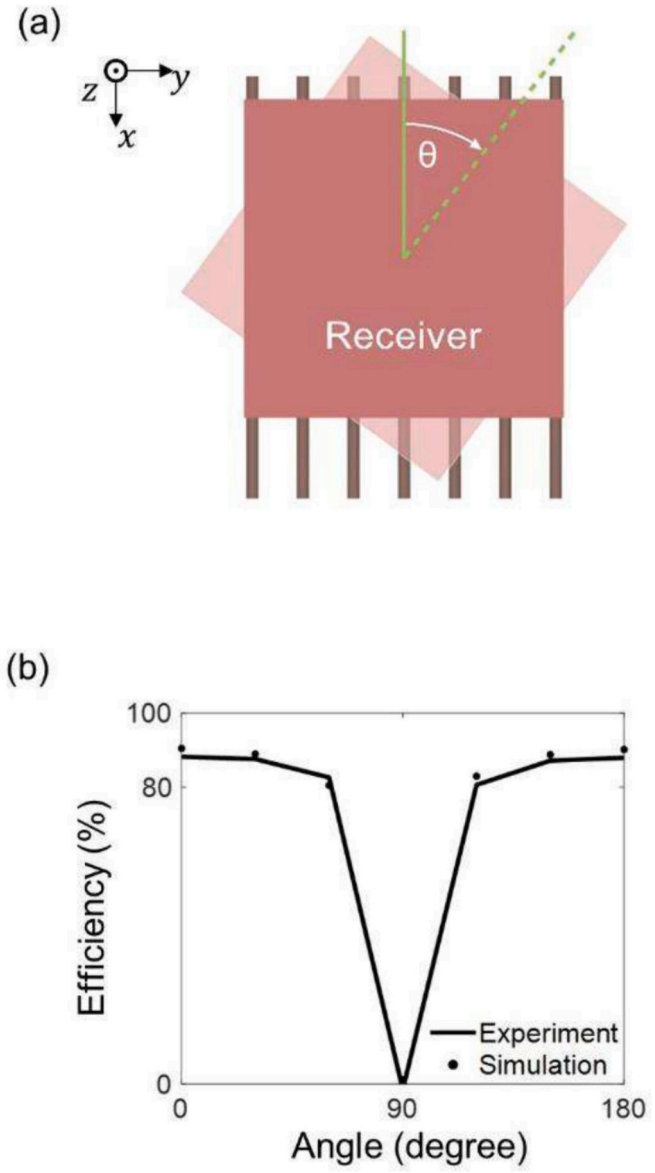

Fig. 14. Validation of angular misalignment tolerance. (a) Visual representation of angular displacement. (b) Simulation and experimental results.

The source power feedback based on the Tx current was verified under the conditions shown in Fig. 17 (a), and the results are shown in Fig. 17 (b). Robot Model 2 was added to the charging track where Robot Model 1 was located. When Robot Model 2 arrived, the Tx current I_p dropped from 9.18 to 8.72 Arms. Simultaneously, the voltage on Robot Model 1 (V_{L1}) decreased, indicating that the pick-up power on Robot Model 1 decreased. After the source power was controlled and I_p rose, V_{L1} escalated, and Robot Model 1 restored the original pick-up power. V_{L2} was also higher than when Robot Model 2 arrived, which means that Robot Model 2 was normally charged in the same track.

5. Safety for co-workers

The purpose of the proposed system is to charge robots operating collaboratively in human-shared spaces. Thus, the system must satisfy the standards for exposure to time-varying electromagnetic fields. In typical environments, physical barriers such as fencing are employed to restrict human access to areas where logistics robots operate. While robots have the capability to stop when they detect obstacles, there is still a risk of injury due to malfunctioning, collisions, or items falling. Therefore, a scenario was established in which the robot approaches a person to hand over an object, and electromagnetic field exposure simulations were conducted. We simulated the propagated electric fields of the system using finite-element analysis software and verified whether the field intensities satisfied the safety level standards approved by the Institute of Electrical and Electronics Engineers (IEEE) [38] and the guidelines provided by the International Commission on Non-ionizing Radiation Protection (ICNIRP) [39].

In the IEEE standard, the electric-field intensity *in situ* (614 V/m) is defined to avoid electrostimulation, which can cause adverse health effects. Similarly, the ICNIRP guidelines limit the internal exposure of the human body (2.7 V/m) (Supporting Note 3). Ansys HFSS v2022.R2 was used for simulation, and the simulation environment was the same as the experimental setting of the optimized system with a single Rx. Simulations were conducted using human models, assuming a worker adjacent to the robot. The material of the vehicle body was set as iron, while that of the wheel was rubber. The electromagnetic properties of the tissues and organs of the human torso and entire body were provided by the finite-element analysis program. Rx with a ferrite core was attached beneath the vehicle, and the material of all the wires was defined as insulated copper. The distance between the vehicle and the human is defined as the length between the closest edges.

Fig. 18 displays the external and internal exposures of co-workers. The internal exposures vary depending on the distance (d) between the robot and human, with the human model positioned at distances ranging from 0 to 50 cm from the robot. The maximum external and internal intensities remained within safety levels, indicating the suitability of the proposed system for workers sharing the workspace. Furthermore, the simulated internal intensities are significantly lower than the safety levels, ensuring that there is no adverse impact on the health of the workers, even when dozens of robots operate in the same space.

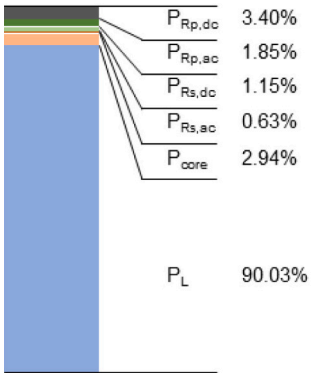

$P_{Rp,dc}$	DC loss (conduction loss) in Tx cable
$P_{Rp,ac}$	AC loss (skin and proximity effect) in Tx cable
$P_{Rs,dc}$	DC loss (conduction loss) in Rx coil
$P_{Rs,ac}$	AC loss (skin and proximity effect) in Rx coil
P_{core}	Core loss (hysteresis, eddy current, and residual loss) in Rx core
P_L	Load power

Fig. 15. Analysis of losses.

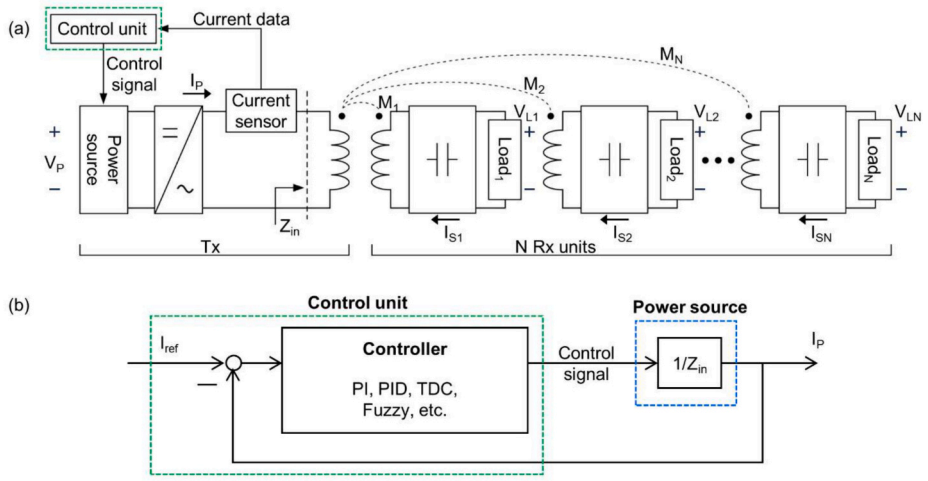

Fig. 16. (a) Circuit model of multiple receivers on the charging track for communication-less power control. (b) A block diagram of the proposed controller.

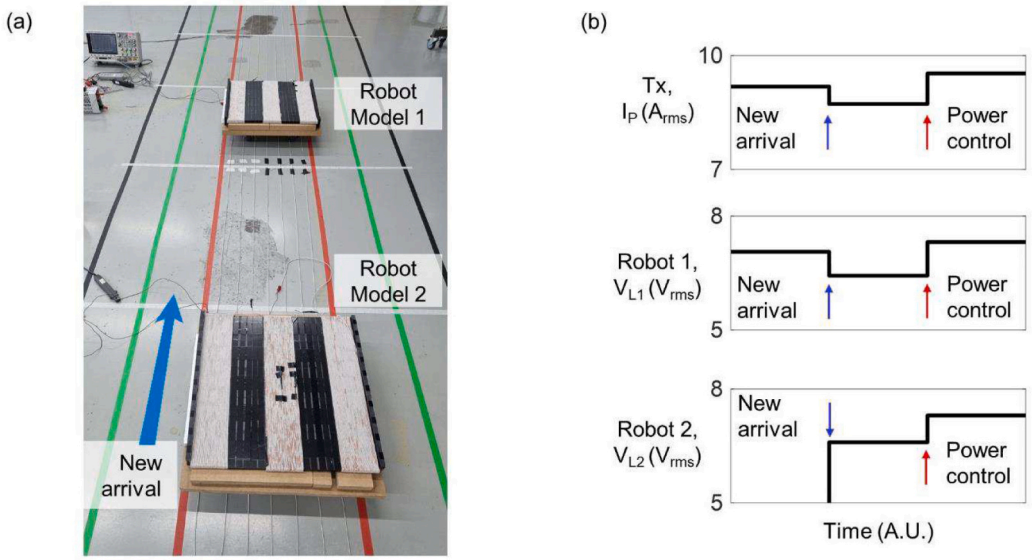

Fig. 17. Communication-less power control for multiple wireless-charging robots. (a) Experimental setup with vehicle models. (b) Results of source power control at the transmitter using reflected impedance.

IEEE and ICNIRP do not enforce regulations on magnetic field intensity for systems that meet the *in situ* electric field strength standards. However, in this study, we have measured the magnetic flux density through experiments to further emphasize the safety of the system and highlight the differences between the proposed system and conventional arrayed solenoid or track type systems. The experimental environment for measuring magnetic flux density can be observed in Fig. 19 (a, b). The setup includes a square track measuring 4 m by 4 m, with a width of 1 m, where the Rx is positioned. Below the Rx, a magnetic field probe (Beehive Electronics LLC, 100C EMC Probe) is placed. This probe is connected to a spectrum analyzer (Agilent Technologies, N9320B) for measuring the magnetic flux density.

The magnetic flux density varied depending on the position of the Rx, but the maximum measured magnetic flux density generated by the Tx was 25.6 uT, which did not exceed the limits set by IEEE and ICNIRP. In the curved sections of the track, we confirmed that the density dropped to about 3/4 of that in the straight segments. However, since the vehicle spends very little time in the curved sections compared to the straight segments, it is not expected to significantly impact the robot's operational performance. Additionally, as the Rx moves away from the track, the measured density decreased sharply, and it was almost non-existent at the center of the track. This is the most significant difference between the proposed system and conventional systems that use flux emanating from the center of a solenoid. Furthermore, the effect of magnetic flux leakage on the metal parts of the robot was demonstrated through a simulation. The leakage induced an electric potential too weak to generate heat, and the results can be found in Supporting Note 4. As a result, simulation and experiments have confirmed that this system does not pose any harm to the human body.

6. Discussion

The global decline in the proportion of the working-age population, as reported by the UN, inevitably necessitates the implementation of mobile robots in various industries. As part of this movement, efforts have been made to charge mobile robots wirelessly. Among these, D-

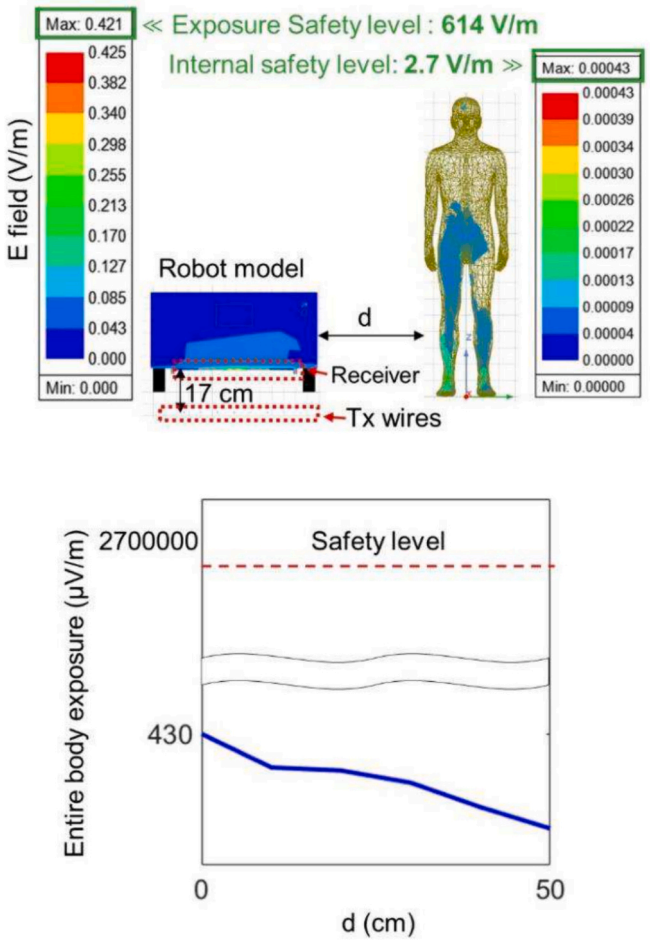

Fig. 18. Simulation results for safety verifications: Exposed electric-field intensities at different distances between the vehicle and worker.

WPT system is a promising technology that enhances robot performance while reducing the cost of robot automation in the industries. Especially, seamless charging, providing uniform power across all DoF of the vehicle, can significantly improve the feasibility of implementing a battery-less mobile robot. By reducing water and energy consumption during the raw material mining process, seamless D-WPT systems are expected to usher in a novel and sustainable approach to energy resource utilization and accelerate the adoption of mobile logistics robots.

This study on the wireless charging track system optimized ferromagnetic-coreless Tx with multiple co-planar wires and Rx with a H-beam structure. Conventional D-WPT systems, which include arrayed solenoids and track types, utilize the z-direction magnetic flux created by merging the flux generated in each segment of the large or small loops comprising the Tx coil. In contrast, the proposed system uses the flux formed in each segment individually for transmitting power. The horizontal magnetic field with strong intensity above the track is adopted to compensate for weak cross-coupling caused by the coreless Tx. While the extended and wide-spread wires ensure constant power against longitudinal and lateral deviations, they pose a challenge during rotation. To address this, additional core legs are introduced to the Rx, making use of the vertical flux aligned with the normal vectors of the core legs.

Consequently, the proposed system provides stable performance to vehicles with any movement in the 3-DoF, with high efficiency of 90%. This is an improvement over other studies that typically offer tolerance in 1- or 2-DoF. Especially, the low fluctuation range of 1% in longitudinal movement makes this technology more promising for dynamic charging for mobile robots. The strength of the system can be demonstrated by a robot driving at a constant speed across the entire track or by comparing its performance with that of a conventional battery-powered robot. Therefore, in future research, we plan to design and conduct experiments with a robot that operates using two actuators. Details about the design can be found in Supporting Note 6.

When more than one vehicle was present on the charging track and a new vehicle arrived, a feedback system without communication with Rx was devised and verified to supply power to all robots appropriately. In addition, for safety, it was confirmed that the exposure of co-workers to the electromagnetic field did not exceed safety limits. In anticipation of the potential large-scale deployment of robots, safety standards permit the simultaneous operation of up to 1458 robots in close proximity to humans. However, maintaining an appropriate distance between humans and robots is crucial to prevent unforeseen accidents. Further research on this matter is expected to proceed through the appropriate Institutional Review Board approval process.

The proposed seamless WPT system is not only applicable to mobile logistics robots but also to common electric mobilities moving on two-dimensional tracks, including bicycles, motorcycles, and cars. However, since this study was conducted at the laboratory level, considering factors such as implementable scale, scenarios, and power, the demonstration focused on showcasing the strengths of seamless charging by applying it to logistics robots. We aim to extend the application of the proposed system to various applications through future research.

When applying the proposed system to different types of vehicles, several considerations must be taken into account to maintain high efficiency: the required power for each application, optimal system design, and the length and shape of the track. The power required for each mobility varies depending on the weight and speed of the vehicle. Additionally, since the electromagnetic field distribution changes based on the space available in the vehicle and the surrounding materials, it is necessary to design a suitable Rx to maintain efficiency. Furthermore, the challenge of decreasing efficiency with increasing transmission distance is a common issue for track type WPT systems. When extending the proposed system to 1 km, we anticipate a maximum efficiency of approximately 80%, which is still competitive with arrayed solenoid systems [27–33]. Especially, considering that switch-based systems may not guarantee both longitudinal and lateral tolerance due to various factors, our proposed system appears promising. Additionally, to cover a large area, it would be efficient to segment the system into appropriate unit lengths. However, allowing the Rx to move between tracks can significantly increase complexity of the system. Thus, further research is needed to deeply investigate which unit structure can cover space most efficiently.

When it comes to the experimental demonstration of the proposed controller, there was a limitation in that the voltage of the power source could only be manually controlled. When manually adjusting the voltage using a variable resistor, the system power had to be turned off for safety reasons, which resulted in data discontinuity and a lack of important performance factors, including response time, overshoot, and steady-state error. Additionally, in the proposed control structure, the focus on eliminating communication has led to a lack of control tailored to the state of each Rx. Therefore, an AI-based Fuzzy algorithm will be adopted in our next study to adjust the received power by changing the Rx's internal resistance when the mutual inductance is sufficient. This addition aims to enhance the system's adaptability and efficiency, ensuring optimal performance for each Rx unit under varying conditions.

The possibility of fracturing in the ferromagnetic material used in the core should be also considered. While still in its early stage, the utilization of organic high-permeability materials [44] or polymer-ferrite composites [45] could present new directions to address these concerns. Additionally, exploring physical solutions such as casing or suspension is a viable option. When it comes to logistics robots, applying them to the field involves flattening the ground, reducing the likelihood of severe vibrations or impacts on the core. However, when

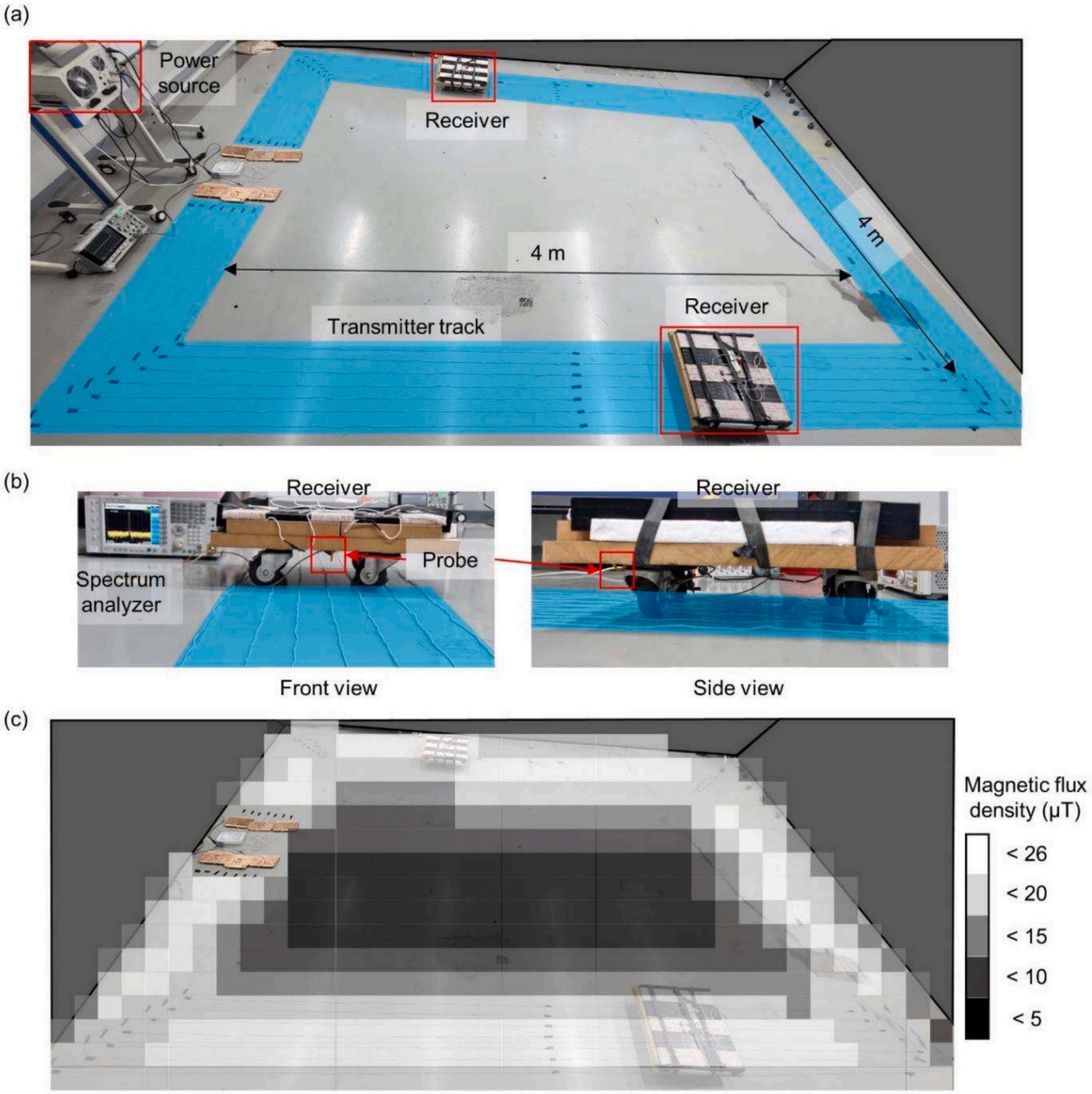

Fig. 19. Experiments measuring magnetic flux density based on receiver position on and around the track. (a, b) Experimental setup. (c) Measured magnetic flux density.

implemented in a real-world environment, vibrational analysis of the natural frequency of the core and vehicle is crucial during the robot design phase. Since this research was conducted in a laboratory setting that cannot fully replicate the complexities of the field environment, field tests under variable load conditions or experiments involving robot models composed of metals and several electronic devices are needed. Furthermore, additional methods such as introducing supplementary couplers, current control, and an impedance matching network could enhance the system to ensure stable power delivery. Nevertheless, this study has implemented and verified the fundamental elements of seamless D-WPT for mobile logistics robots, and it is expected to lead to innovations in industries.

CRediT authorship contribution statement

Hyunkyeong Jo: Writing – review & editing, Writing – original draft, Visualization, Validation, Software, Project administration, Methodology, Investigation, Formal analysis, Data curation, Conceptualization. **Seoktae Seo:** Writing – review & editing, Writing – original draft, Visualization, Validation, Software, Investigation. **Jungho Kim:** Writing – review & editing, Investigation. **Franklin Bien:** Writing – review & editing, Supervision, Resources, Funding acquisition.

Declaration of competing interest

The authors declare that they have no known competing financial interests or personal relationships that could have appeared to influence the work reported in this paper.

Data availability

Data will be made available on request.

Acknowledgements

This research was supported by the Ministry of Science and ICT, South Korea (Grant Numbers: IITP-2022-RS-2022-00156361, NRF-2017R1A5A1015596).

Appendix A. Supplementary data

Supplementary data to this article can be found online at https://doi.org/10.1016/j.apenergy.2024.123943.

References

[1] Ballestar MT, Díaz-Chao A, Sainz J, Torrent-Sellens J. Knowledge, robots and productivity in SMEs: explaining the second digital wave. J Bus Res 2020;108:119–31. https://doi.org/10.1016/j.jbusres.2019.11.017.

[2] Loganathan A, Ahmad NS. A systematic review on recent advances in autonomous mobile robot navigation. Eng Sci Technol an Int J 2023;40:101343. https://doi.org/10.1016/j.jestch.2023.101343.

[3] Bechtsis D, Tsolakis N, Vlachos D, Iakovou E. Sustainable supply chain management in the digitalisation era: the impact of automated guided vehicles. J Clean Prod 2017;142(4):3970–84. https://doi.org/10.1016/j.jclepro.2016.10.057.

[4] Zhang J, Yang X, Wang W, Guan J, Ding L, Lee VCS. Automated guided vehicles and autonomous mobile robots for recognition and tracking in civil engineering. Autom 2023;146:104699. https://doi.org/10.1016/j.autcon.2022.104699.

[5] Farooq MU, Eizad A, Bae H. Power solutions for autonomous mobile robots: a survey. Robot Auton Syst ;159:104285. https://doi.org/10.1016/j.robot.2022.104285.

[6] Seo S, Jo H, Bien F. Free arrangement wireless power transfer system with a ferrite transmission medium and geometry-based performance improvement. IEEE Trans Power Electron 2020;35(5):4518–32. https://doi.org/10.1109/TPEL.2019.2945532.

[7] Gong W, Xiao J, Han S, Wu X, Wu N, Chen S. Research on robot wireless charging system based on constant-voltage and constant-current mode switching. Energy Rep 2022;8:940–8. https://doi.org/10.1016/j.egyr.2022.02.025.

[8] Lu F, Zhang H, Hofmann H, Mi CC. A dynamic charging system with reduced output power pulsation for electric vehicles. IEEE Trans Ind Electron 2016;63(10):6580–90. https://doi.org/10.1109/TIE.2016.2563380.

[9] Zhao L, Thrimawithana DJ, Madawala UK. Hybrid bidirectional wireless EV charging system tolerant to pad misalignment. IEEE Trans Ind Electron 2017;64(9):7079–86. https://doi.org/10.1109/TIE.2017.2686301.

[10] Chen Y, Yang B, Zhou X, Li Q, He Z, Mai R, et al. A hybrid inductive power transfer system with misalignment tolerance using quadruple-D quadrature pads. IEEE Trans Power Electron 2020;35(6):6039–49. https://doi.org/10.1109/TPEL.2019.2954906.

[11] Song K, Yang G, Guo Y, Lan Y, Dong S, Jiang J, et al. Design of DD coil with high misalignment tolerance and low EMF emissions for wireless electric vehicle charging systems. IEEE Trans Power Electron 2020;35(9):9034–45. https://doi.org/10.1109/TPEL.2020.2971967.

[12] Mai J, Wang Y, Yao Y, Sun M, Xu D. High-misalignment-tolerant IPT systems with solenoid and double D pads. IEEE Trans Ind Electron 2022;69(4):3527–35. https://doi.org/10.1109/TIE.2021.3075841.

[13] Zhang C, Lu W, Zhao J, Wu X, Chen H, Xu D. A novel asymmetric magnetic coupler applied to multiple-receiver wireless charging system for automated guided vehicles. IEEE Trans Power Electron 2023;38(11):14761–75. https://doi.org/10.1109/TPEL.2023.3307461.

[14] Xia C, Wang W, Ren S, Wu W, Sun Y. Robust control for inductively coupled power transfer systems with coil misalignment. IEEE Trans on Power Electron 2018;33(9):8110–22. https://doi.org/10.1109/TPEL.2017.2771532.

[15] Wijaya FP, Shimotsu T, Saito T, Kondo K. A simple active power control for a high-power wireless power transmission system considering coil misalignment and its design method. IEEE Trans Power Electron 2018;33(11):9989–10002. https://doi.org/10.1109/TPEL.2018.2799679.

[16] Lee T, Huang S, Dai S, Su J. Design of misalignment-insensitive inductive power transfer via interoperable coil module and dynamic power control. IEEE Trans Power Electron 2020;35(9):9024–33. https://doi.org/10.1109/TPEL.2020.2972035.

[17] Ahmad A, Alam MS, Rafat Y, Shariff S. Designing and demonstration of misalignment reduction for wireless charging of autonomous electric vehicle. eTransportation 2020;4:100052. https://doi.org/10.1016/j.etran.2020.100052.

[18] Mai J, Wang Y, Yao Y, Xu D. Analysis and design of high-misalignment-tolerant compensation topologies with constant-current or constant-voltage output for IPT systems. IEEE Trans Power Electron 2020;36(3):2685–95. https://doi.org/10.1109/TPEL.2020.3014687.

[19] Shi B, Yang F, Hu C, Ouyang M. Modelling and improvement of oscillation problem in a double-sided LCC compensation network for electric vehicle wireless power transfer. eTransportation 2021;8:100108. https://doi.org/10.1016/j.etran.2021.100108.

[20] Zhang Y, Pan W, Wang H, Shen Z, Wu Y, Dong J, et al. Misalignment-tolerant dual-transmitter electric vehicle wireless charging system with reconfigurable topologies. IEEE Trans Power Electron 2022;37(8):8816–9. https://doi.org/10.1109/TPEL.2022.3160868.

[21] Lukic S, Pantic Z. Cutting the cord: static and dynamic inductive wireless charging of electric vehicles. IEEE Electrific Mag 2013;1(1):57–64.

[22] Chopra S, Bauer P. Driving range extension of EV with on-road contactless power transfer—a case study. IEEE Trans Ind Electron 2013;60(1):329–38.

[23] Chen Z, He F, Yin Y. Optimal deployment of charging lanes for electric vehicles in transportation networks. Transp Res B Methodol 2016;91:344–65.

[24] Jeong S, Jang YJ, Kum D, Lee MS. Charging automation for electric vehicles: is a smaller battery good for the wireless charging electric vehicles? IEEE Trans Autom Sci Eng 2019;16(1):486–97. https://doi.org/10.1109/TASE.2018.2827954.

[25] Herrington R. Mining our green future. Nat Rev Mater 2021;6:456–8. https://doi.org/10.1038/s41578-021-00325-9.

[26] Feng H, Tavakoli R, Onar OC, Pantic Z. Advances in high-power wireless charging systems: overview and design considerations. IEEE Trans Transp Electrification 2020;6(3):886–919. https://doi.org/10.1109/TTE.2020.3012543.

[27] Zhou S, Mi CC. Multi-paralleled LCC reactive power compensation networks and their tuning method for electric vehicle dynamic wireless charging. IEEE Trans Ind Electron 2016;63(10):6546–56. https://doi.org/10.1109/TIE.2015.2512236.

[28] Huang S, Lee T, Li W, Chen R. Modular on-road AGV wireless charging systems via interoperable power adjustment. IEEE Trans Ind Electron 2019;66(8):5918–28. https://doi.org/10.1109/TIE.2018.2873165.

[29] Lu F, Zhang H, Hofmann H, Mi CC. A dynamic charging system with reduced output power pulsation for electric vehicles. IEEE Trans Ind Electron 2016;63(10):6580–90. https://doi.org/10.1109/TIE.2016.2563380.

[30] Li Y, Hu J, Lin T, Li X, Chen F, He Z, et al. A new coil structure and its optimization design with constant output voltage and constant output current for electric vehicle dynamic wireless charging. IEEE Trans Ind Inform 2019;15(9):5244–56. https://doi.org/10.1109/TII.2019.2896358.

[31] Li X, Hu J, Wang H, Dai X, Sun Y. A new coupling structure and position detection method for segmented control dynamic wireless power transfer systems. IEEE Trans Power Electron 2020;35(7):6741–5. https://doi.org/10.1109/TPEL.2019.2963438.

[32] Cai C, Saeedifard M, Wang J, Zhang P, Zhao J, Hong Y. A cost-effective segmented dynamic wireless charging system with stable efficiency and output power. IEEE Trans Power Electron 2022;37(7):8682–700. https://doi.org/10.1109/TPEL.2022.3143128.

[33] Kanazawa H, Uwai H, Kiuchi S, Matsumoto H. Receiver-position-based unbalanced-current control for a three- to single-phase wireless power transfer system for AGVs. IEEE Trans Ind Electron 2023;70(4):3245–56. https://doi.org/10.1109/TIE.2022.3177799.

[34] Huh J, Lee SW, Lee WY, Cho GH, Rim CT. Narrow-width inductive power transfer system for online electrical vehicles. IEEE Trans Power Electron 2011;26(12):3666–79. https://doi.org/10.1109/TPEL.2011.2160972.

[35] Kissin MLG, Covic GA, Boys JT. Steady-state flat-pickup loading effects in polyphase inductive power transfer systems. IEEE Trans Ind Electron 2011;58(6):2274–82. https://doi.org/10.1109/TIE.2010.2060455.

[36] Raabe S, Covic GA. Practical design considerations for contactless power transfer quadrature pick-ups. IEEE Trans Ind Electron 2013;60(1):400–9. https://doi.org/10.1109/TIE.2011.2165461.

[37] Choi SY, Jeong SY, Gu BW, Lim GC, Rim CT. Ultraslim S-type power supply rails for roadway-powered electric vehicles. IEEE Trans Power Electron 2015;30(11):6456–68. https://doi.org/10.1109/TPEL.2015.2444894.

[38] TC95. IEEE SCC39 International Committee on Electromagnetic Safety (ICES). PC95.1TM/D3.5 Draft standard for safety levels with respect to human exposure to electric, magnetic and electromagnetic fields, 0 Hz to 300 GHz. IEEE-SA Standards Board 2018:1–62.

[39] International Commission on Non-Ionizing Radiation Protection (ICNIRP). Guidelines for limiting exposure to time-varying electric and magnetic fields (1 Hz to 100 kHz). Health Phys 2010;99(6):818–36.

[40] International Telecommunication Union (ITU). Guidance on frequency ranges for operation of non-beam wireless power transmission for electric vehicles. Recommendation ITU-R SM.2110–1. 2019. 1–6.

[41] Shevchenko V, Husev O, Strzelecki R, Pakhaliuk B, Poliakov N, Strzelecka N. Compensation topologies in IPT systems: standards, requirements, classification, analysis, comparison and application. IEEE Access 2019;7:120559–80. https://doi.org/10.1109/ACCESS.2019.2937891.

[42] Dowell PL. Effects on eddy currents in transformer windings. Proc IEEE 1966;133:1–16.

[43] Smith GS. Proximity effect in Systems of Parallel Conductors. J Appl Phys 1972;43(5):2196–203. https://doi.org/10.1063/1.1661474.

[44] Mahmood J, et al. Organic ferromagnetism: trapping spins in the glassy state of an organic network structure. Chem 2018;4(10):2357–69.

[45] Dosoudil R, Usakova M, Franek J, Slama J, Gruskova A. Particle size and concentration effect on permeability and EM-wave absorption properties of hybrid ferrite polymer composites. IEEE Trans Magn 2010;46(2):436–9. https://doi.org/10.1109/TMAG.2009.2033347.